PNAS
www.pnas.org

Supplementary Information for

Temperature and rigidity mediated rapid transport of lipid nanovesicles in hydrogels

Miaorong Yu, Wenyi Song, Falin Tian, Zhuo Dai, Quanlei Zhu, Ejaj Ahmad, Shiyan Guo, Chunliu Zhu, Haijun Zhong, Yongchun Yuan, Tao Zhang, Xin Yi, Xinghua Shi, Yong Gan, Huajian Gao

Corresponding Authors: Xinghua Shi, shixh@nanoctr.cn; Yong Gan, ygan@simm.ac.cn; Huajian Gao, huajian_gao@brown.edu

This PDF file includes:

Figs. S1 to S15
Tables S1 to S5
Captions for movies S1 to S6
References for SI reference citations

Other supplementary materials for this manuscript include the following:

Movies S1 to S6

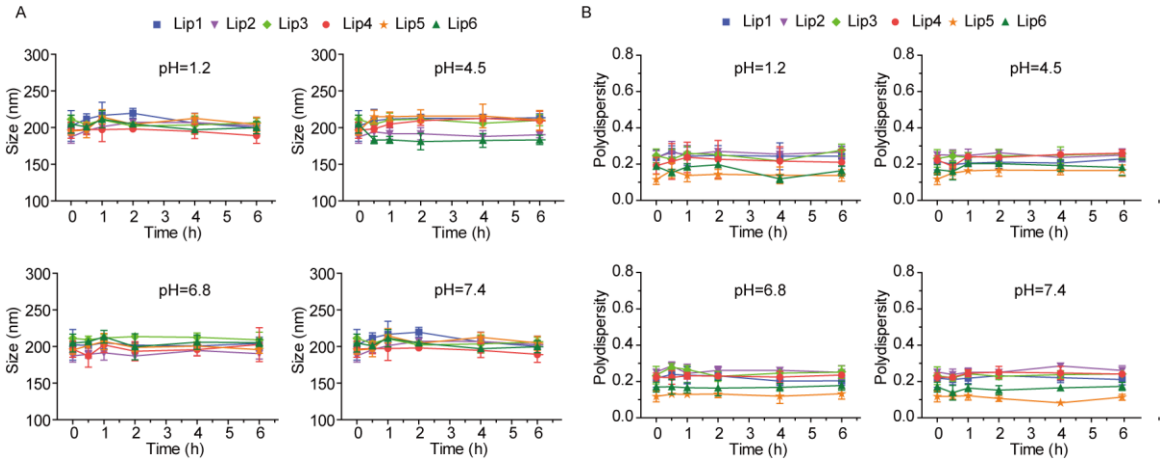

Fig. S1. Stability of the liposomes. Size (A) and polydispersity (PDI) (B) of the liposomes after 6 h in different media at 37 °C. Data are shown as the means ± SD with n=3.

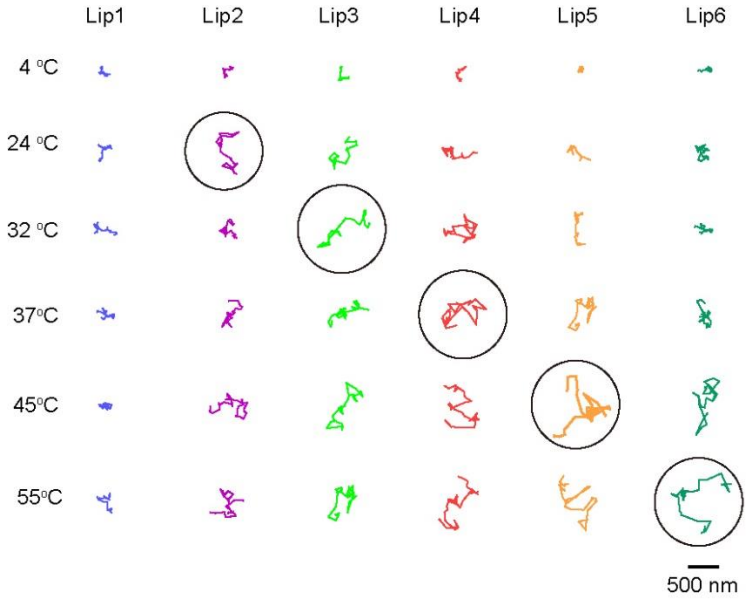

Fig. S2. Representative trajectories of liposomal motion in PEO hydrogels in 1 s at different temperatures.

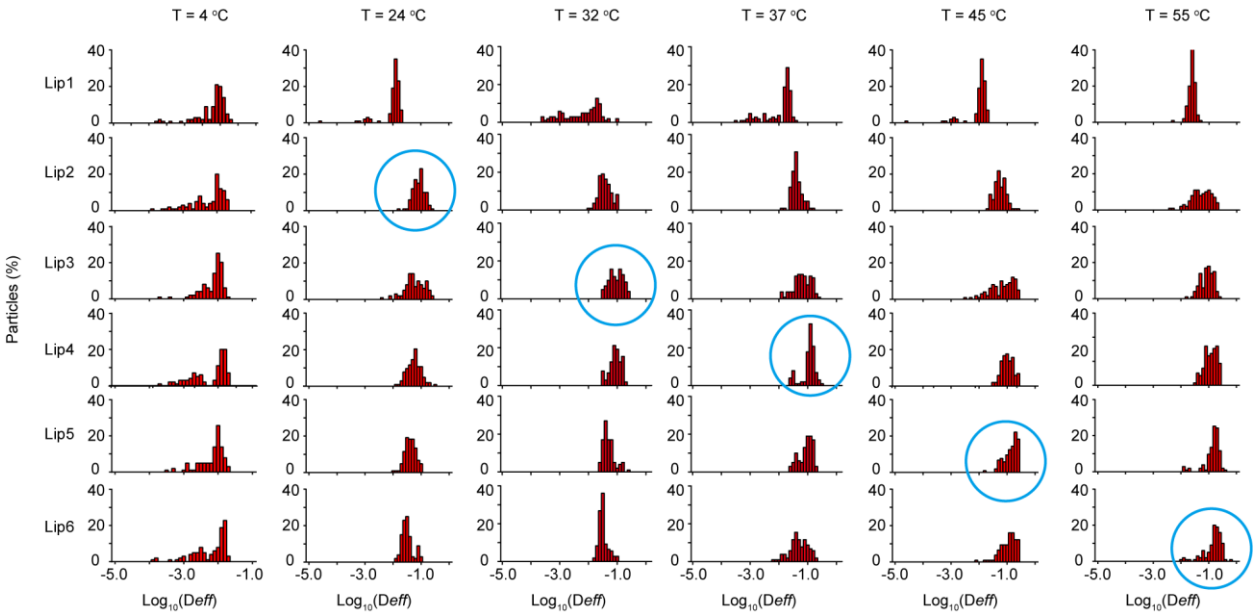

Fig. S3. Distribution of the logarithms of individual particle effective diffusivities (D_{eff}) on a time scale of 1 s in PEO hydrogels at different temperatures.

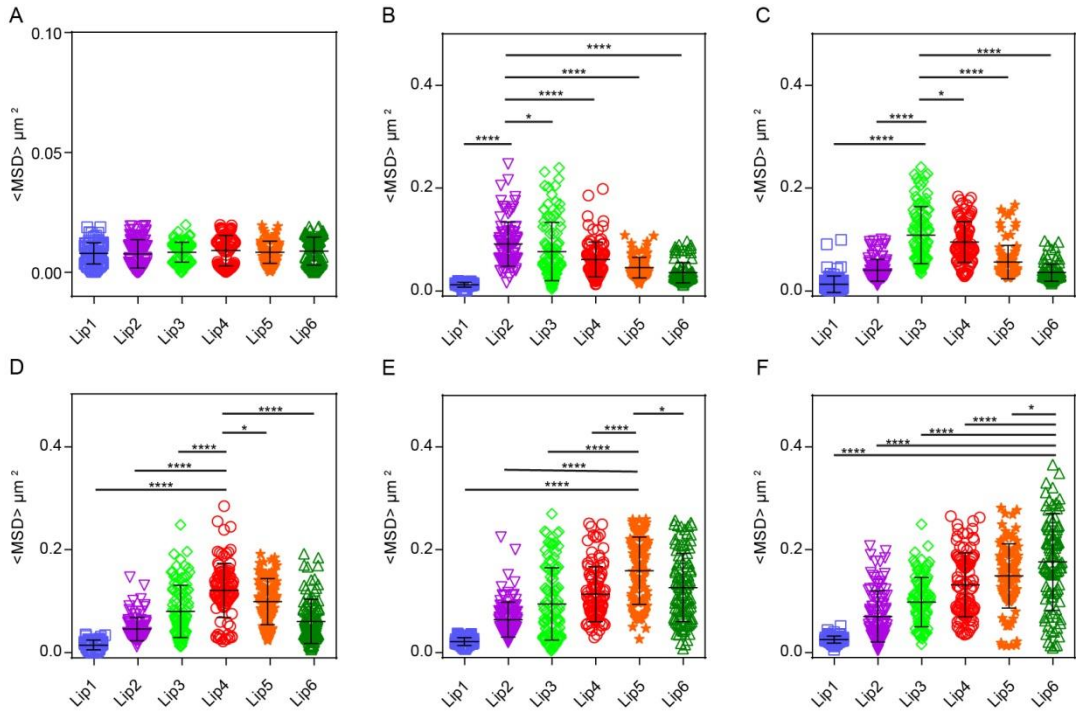

Fig. S4. Mobility of liposomes in PEO hydrogel at different temperatures. Typical MSD values for liposomes in 1 s at (A) 4 °C, (B) 24 °C, (C) 32 °C, (D) 37 °C, (E) 45 °C and (F) 55 °C, respectively. The data represent three independent experiments, and each

experiment tracks 100 particles. The data are shown as the means ±SD (n = 3). *P < 0.05, ****P < 0.0001.

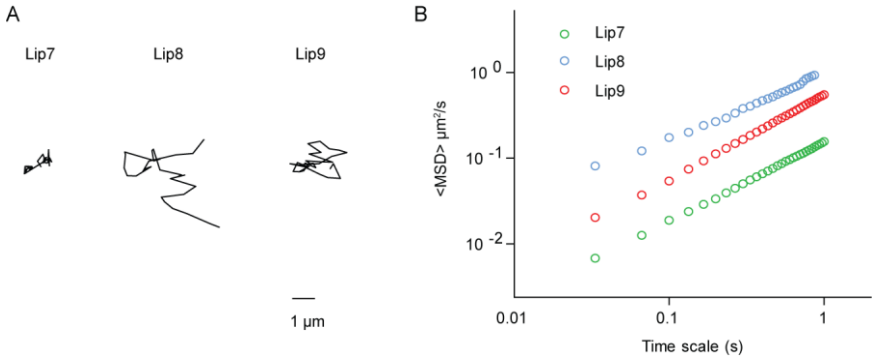

Fig. S5. Characterizations of the diffusivity of liposomes with different compositions in rat intestinal mucus. (A) Representative trajectories and (B) MSD of the logarithms of effective diffusivities (D_{eff}) of liposome motion in 1 s at 37 °C. The data represent three independent experiments, and each experiment tracks 100 particles.

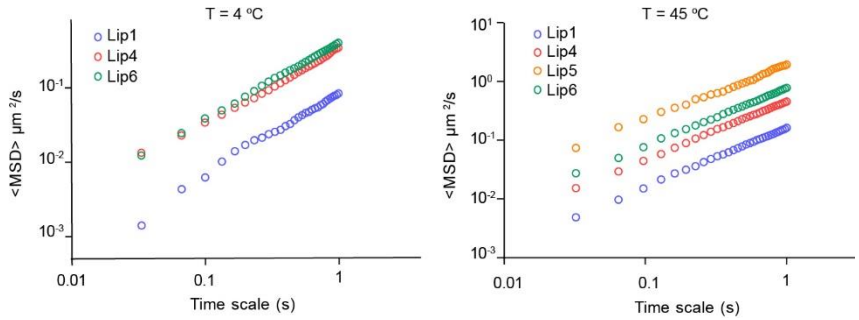

Fig. S6. The diffusivity of liposomes in rat intestinal mucus at 4 and 45 °C. MSD of the logarithms of effective diffusivities (D_{eff}) of liposome motion in 1 s at 4 and 45 °C. The data represent three independent experiments, and each experiment tracks 100 particles.

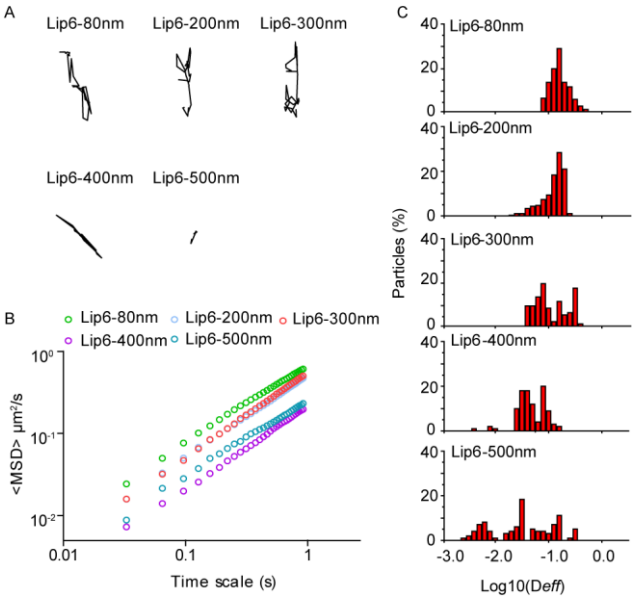

Fig. S7. Transport of Lip6 with different sizes (80, 200, 300, 400 and 500 nm) in fresh rat intestinal mucus at 37 °C. (A) Representative trajectories of particle motion in 1 s. (B) MSD values as a function of time. (C) Distribution of the logarithms of individual particle effective diffusivities (D_{eff}) on a time scale of 1 s. The data represent three independent experiments, and each experiment tracks 100 particles.

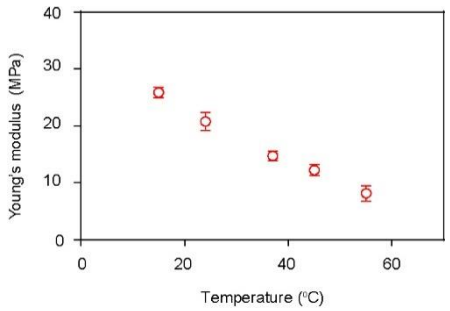

Fig. S8. The Young's moduli of Lip4 characterized by AFM at different temperatures. The data represent three independent experiments.

Simulation model and method. Similar to our previous study, a regular polymer network was utilized to represent mucus fibers with a mesh size of 42σ, as shown in Fig. S9. Each fiber comprised a series of beads spanning the entire simulation box ($168 \times 168 \times 168\sigma^3$). Different fibers were cross-linked by a node bead to simulate the entanglement and crosslinking of mucin fibers. The bonded interaction energy

between neighboured beads *i* and *j* in the polymer chain was described by a simple harmonic spring with a spring constant of $k_b = 23\,\varepsilon/\sigma^2$ and an equilibrium bond length of $r_0 = 2.0\sigma$

$$E_{bond} = \frac{1}{2}k_b(r - r_0)^2 \quad \text{(S1)}$$

The energy constraining the bond angle was described by an equilibrium angle with a bending constant of $k_a = 4.6\varepsilon$ and an equilibrium bond angle of $\theta_0 = \pi$

$$E_{angle} = \frac{1}{2}k_a(\theta - \theta_0)^2 \quad \text{(S2)}$$

During the simulations, polymer node beads were constrained by applying a spring to tether them to their initial positions. The spring constant was set to $k_{self} = 4.6\,\varepsilon/\sigma^2$. The Lennard-Jones (LJ) potential was used as follows to describe the nonbonded interactions $V(r_{ij})$ between two beads

$$V(r_{ij}) = 4\varepsilon_{ij}\left[\left(\frac{b}{r_{ij}}\right)^{12} - \left(\frac{b}{r_{ij}}\right)^{6}\right] \qquad r_{ij} < r_c \quad \text{(S3)}$$

where ε_{ij} is the depth of the energy well, b is the equilibrium length between two beads, and r_c is the cut-off distance. The interaction parameters are listed in Table S4. The polymer network was constructed using 3904 beads, 4032 bonds and 4032 angles. The water molecule was represented by one CG bead. In the simulation, each liposome contained 796 water beads in the inner liposome, and the other 212,863 water beads were used to fill the simulation box.

The liposome with a size of 42σ was modeled using the one-particle-thick model, which captures liposome elastic properties, to allow the stiffness tuning of the liposomes. Each type of liposome comprised 3155 beads. Following the notation from the original paper, the interparticle interaction between each pair of liposome beads was described by a combination of two functions, $\mathrm{u}(r)$ and $\phi(\hat{\mathbf{r}}_{ij}, \mathbf{n}_i, \mathbf{n}_j)$, which represent the distance and orientation dependences, respectively, as follows:

$$U(\mathbf{r}_{ij}, \mathbf{n}_i, \mathbf{n}_j) = \begin{cases} u_R(r) + \varepsilon_{beads-beads}\left[1 - \phi(\hat{\mathbf{r}}_{ij}, \mathbf{n}_i, \mathbf{n}_j)\right] & r < r_{min} \\ u_A(r)\phi(\hat{\mathbf{r}}_{ij}, \mathbf{n}_i, \mathbf{n}_j) & r_{min} < r < r_c \end{cases} \quad \text{(S4)}$$

Where

$$u_A(r) = -\varepsilon_{beads-beads}\cos^{2\zeta}\left(\frac{\pi}{2}\frac{r-r_{min}}{r_c-r_{min}}\right) \quad r_{min} < r < r_c \tag{S5}$$

$$u_R(r) = \varepsilon_{beads-beads}\left[\left(\frac{r_{min}}{r}\right)^4 - 2\left(\frac{r_{min}}{r}\right)^2\right] \quad r < r_{min} \tag{S6}$$

$$\phi(\hat{\mathbf{r}}_{ij}, \mathbf{n}_i, \mathbf{n}_j) = 1 + \mu\left(a(\hat{\mathbf{r}}_{ij}, \mathbf{n}_i, \mathbf{n}_j) - 1\right) \tag{S7}$$

$$a(\hat{\mathbf{r}}_{ij}, \mathbf{n}_i, \mathbf{n}_j) = (\mathbf{n}_i \times \hat{\mathbf{r}}_{ij}) \cdot (\mathbf{n}_j \times \hat{\mathbf{r}}_{ij}) + \sin\theta_0(\mathbf{n}_i - \mathbf{n}_j) \cdot \hat{\mathbf{r}}_{ij} - \sin^2\theta_0 \tag{S8}$$

In these equations $\mathbf{r}_i$ and $\mathbf{r}_j$ represent the center position vectors of beads *i* and *j*, $\mathbf{r}_{ij} = \mathbf{r}_i - \mathbf{r}_j$, r=$\|\mathbf{r}_{ij}\|$ and $\hat{\mathbf{r}}_{ij} = \mathbf{r}_{ij}/r$. The unit vectors $\mathbf{n}_i$ and $\mathbf{n}_j$ represent the axes of symmetry of beads *i* and *j*, respectively. The exponent ζ tuned the slope of the attraction between two beads. The parameters θ_0 and μ were related to the spontaneous curvature and bending rigidity of the liposomes. In the simulations, we chose the same parameters $\varepsilon_{beads-beads} = 1\varepsilon$, $\zeta = 4$, and $r_c = 2.6\sigma$ as used in the original paper. The other two parameters (μ, $\sin\theta_0$) were used to modify the bending rigidity of different types of liposomes and are listed in Table S5. The interaction potential for the liposome-polymer network and liposome-liposome interactions was also described by the LJ potential. The interaction between different liposomes is zero, and the interaction parameters are listed in Table S4.

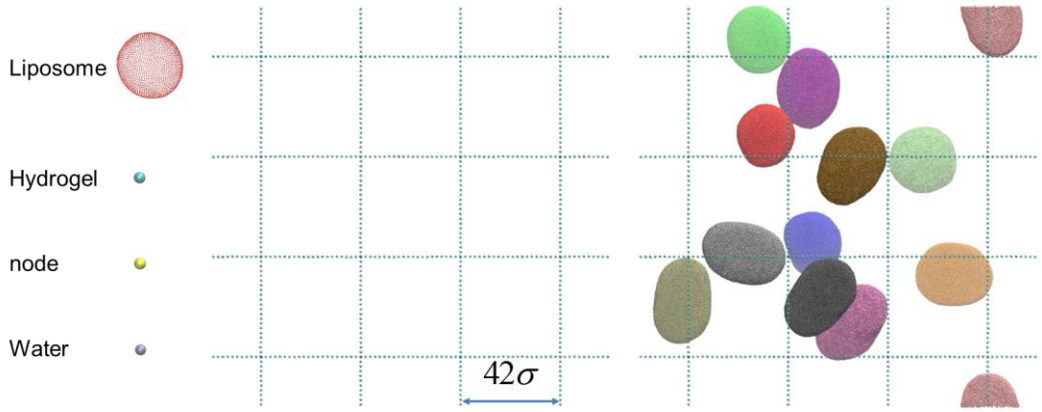

Fig. S9. The coarse-grained model for the diffusion of liposomes in our simulations and a typical snapshot of the simulation system. The regular hydrogel network was utilized to represent mucus fibers with a mesh size of 42σ. Liposomes are modeled using the one-particle-thick model with an initial diameter of 30σ.

Simulation temperature and liposome rigidity. In our coarse-grained simulations, different simulation temperatures and liposomes with various T_m were chosen to investigate the effect of T_m of liposome on their diffusivity. As reported by the original paper (1), the fluidity of the vesicle varied with the parameter ζ and temperature (Fig. S10A), which will change from the gel to fluid phase when the temperature increases with a fixed ζ. In other words, by changing the simulation temperature, different phase of liposome can be obtained. In this model, the bending rigidity of the vesicle increased with μ monotonically (Fig. S10B). In addition, the spontaneous curvature per bead can be implemented via the parameter θ_0. Therefore, we can obtain liposomes with different fluidities via tuning the simulation temperature, μ and θ_0 at fixed $\zeta = 4$. For example, from Fig. S10a we can see that the gel-fluid transition temperature is $k_BT = 0.15\varepsilon$ for $\mu = 3$ and θ_0 =0. Thus, we chose the parameters $\mu = 3$ and θ_0 =0 for the liposome with lowest T_m. Similarly, the parameters for the other two types of liposomes and simulation temperatures were selected based on the same strategy.

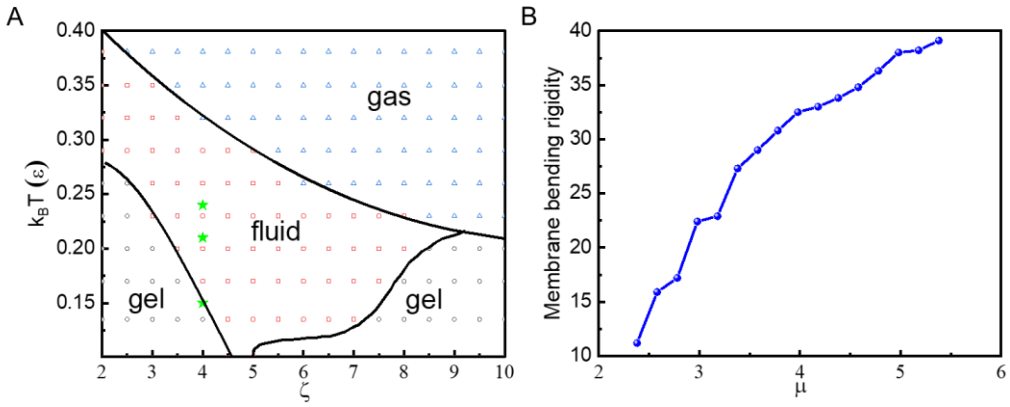

Fig. S10. The phase-diagram in the (ζ, T) plane (A) and membrane bending rigidity varies with μ of the coarse-grained vesicle models at zero tension (B). (A) Three regions representing gel (black circle), fluid (red square), and gas (blue triangle) phases are identified, separated by solid lines. The green stars represent three simulation temperature in the simulation. (B) Membrane bending rigidity monotonically increases with μ. The parameters used are $\zeta = 4$, θ_0 =0, $k_BT = 0.23\varepsilon$.

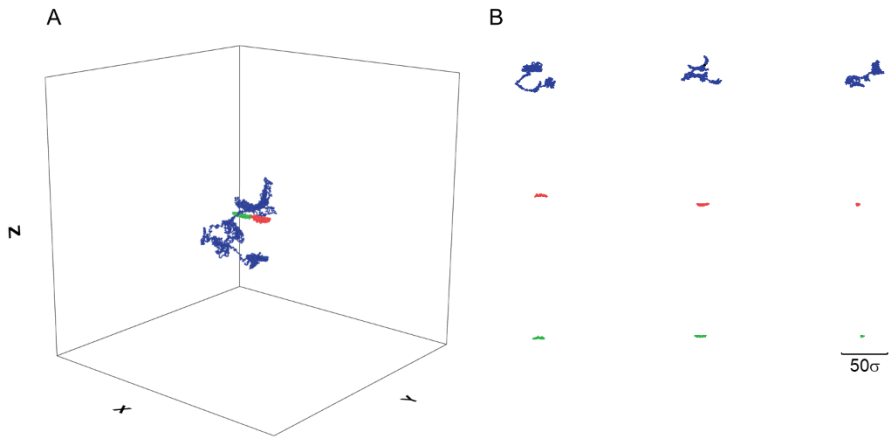

Fig. S11. The typical 3D centroid trajectories of liposomal in simulation (A) and their corresponding projection in different 2D plane (B) at T*=0.15ε. From left to right are projections of centroid trajectories in XY-plane, XZ-plane, YZ-plane in (B). The blue, red, and green labels correspond to liposomes with low T_m, intermediate T_m, and high T_m, respectively. Low T_m: Lip1; Intermediate T_m: Lip4; High T_m: Lip6.

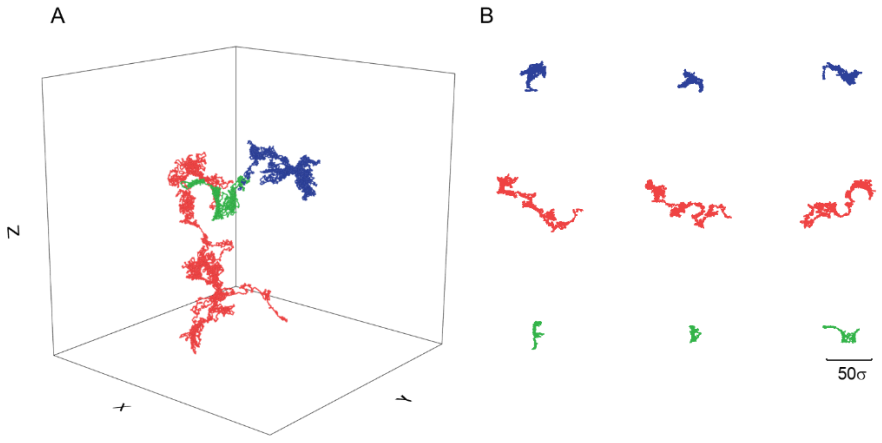

Fig. S12. The typical 3D centroid trajectories of liposomal in simulation (A) and their corresponding projection in different 2D plane (B) at T*=0.21ε. From left to right are projections of centroid trajectories in XY-plane, XZ-plane, YZ-plane in (B). The blue, red, and green labels correspond to liposomes with low T_m, intermediate T_m,

and high T_m, respectively. Low T_m: Lip1; Intermediate T_m: Lip4; High T_m: Lip6.

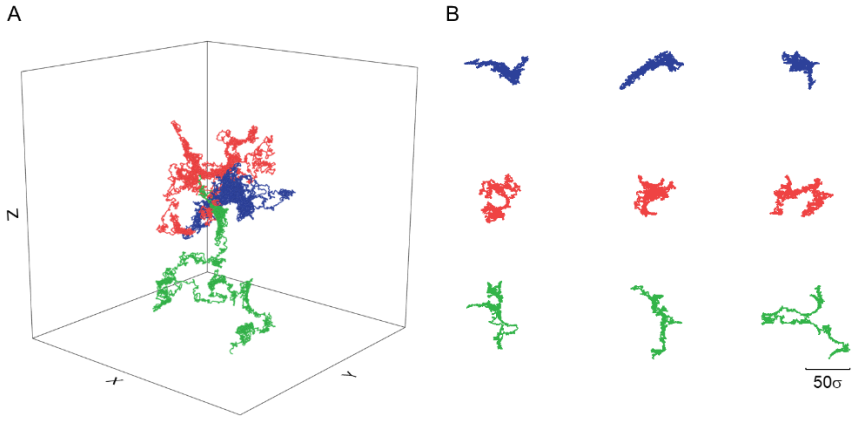

Fig. S13. The typical 3D centroid trajectories of liposomal in simulation (A) and their corresponding projection in different 2D plane (B) at T*=0.24ε. From left to right are projections of centroid trajectories in XY-plane, XZ-plane, YZ-plane in (B). The blue, red, and green labels correspond to liposomes with low T_m, intermediate T_m, and high T_m, respectively. Low T_m: Lip1; Intermediate T_m: Lip4; High T_m: Lip6.

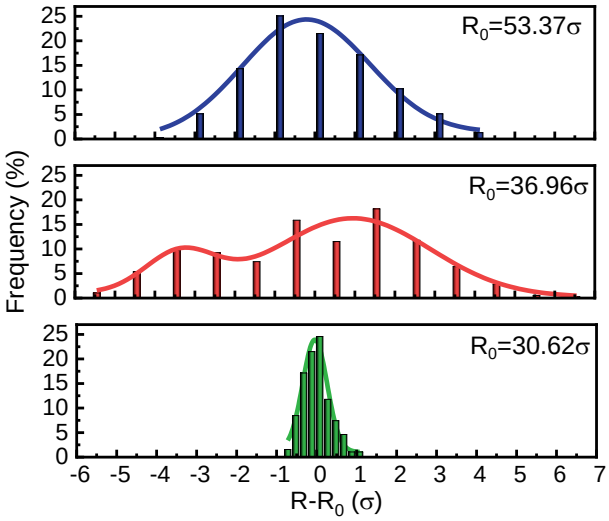

Fig. S14. Distribution of the fluctuation in length of the major axis of liposomes around the time averaged value R_0. The blue, red, and green labels correspond to

liposomes with low T_m, intermediate T_m, and high T_m, respectively. Low T_m: Lip1; Intermediate T_m: Lip4; High T_m: Lip6. The simulation temperature is taken as $T^*=0.21\varepsilon$.

Effect of the pore size of the polymer network

It has been reported that the mesh size of mucus varies in a wide range of 10-1000 nm. In our experiment, we found that the average pore size of the mucus is about 100-240 nm, and the hydrodynamic diameter of the liposomes has a comparable value of about 200 nm. To mimic these experimental size scales, we set the ratio of the liposome size and network mesh pore size to be 30:42. In addition, we have studied a system with a decreased pore size of 35σ, in which case almost all the liposomes were trapped in the network within one grid cell (Fig. S15A-B). We also increased the pore size to 50σ, and observed an increase in diffusivity due to loosened restrictions of the mucus network compared to those with a smaller pore size (35σ) (Fig. S15C-D). Similarly, the liposome diffused faster at $T^* = 0.21\varepsilon$ than those at $T^* = 0.15\varepsilon$ and $T^* = 0.24\varepsilon$ (Fig. S15C-D).

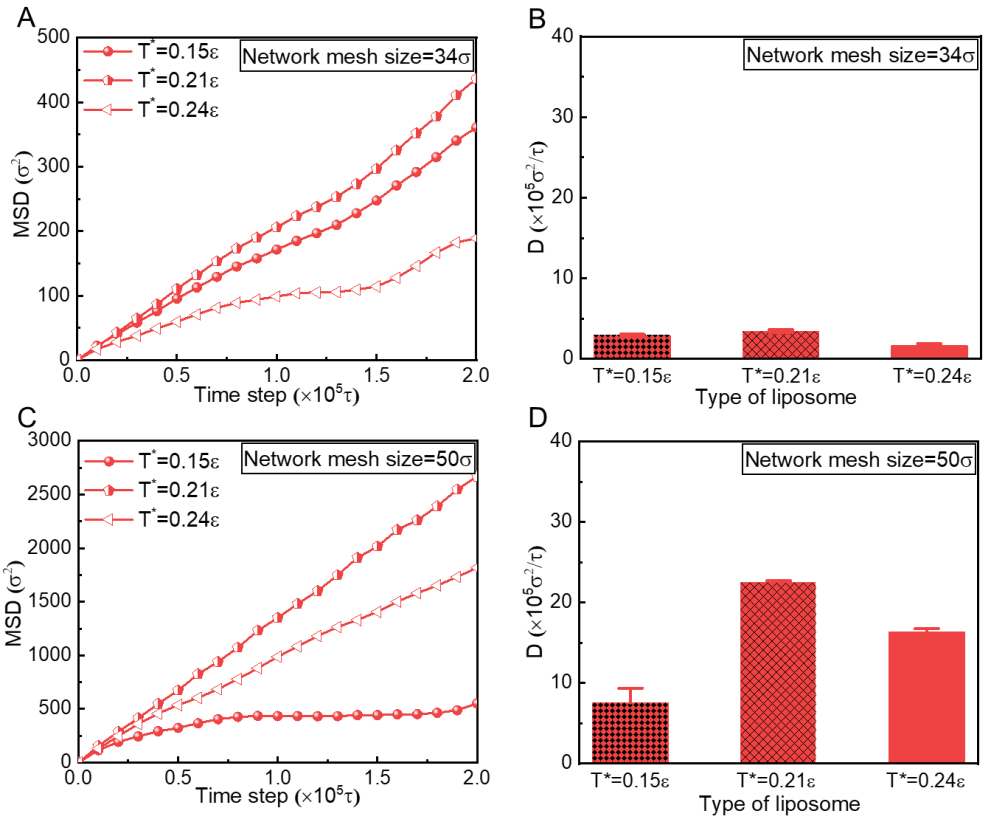

Fig. S15. Effect of mucus pore size on the diffusion of liposomes. The (A & C) MSDs and (B & D) diffusivities of liposomes when the pore size of the mucus network is tuned from 42σ to 35σ or 50σ. The solid sphere line, semi-solid pentagon line, and hollow triangle line in (A) and (C) correspond to the simulation temperatures of $T^* = 0.15\varepsilon$, $T^* = 0.21\varepsilon$, and $T^* = 0.24\varepsilon$, respectively. During the simulations, the paramaters of the liposomes are taken as: $\mu = 5$ and $sin\theta = 0.002$, corresponding to the liposome with intermediate T_m.

Tables

Table S1. Characterization of the liposomes and their diffusivities in rat intestinal mucus

Sample	Composition	Hydrodynamic diameter (nm)	PDI	Zeta potential (mV)	Diffusivity ($\mu m^2/s$)	T_m (°C)
Lip1	DOPE:DOPE-PEG_{2000} 95%：5%	184.0 ± 9.8	0.147	-2.9 ± 2.3	0.126	-16.0
Lip2	DMPC:DSPE-PEG_{2000} 95%：5%	203.6 ± 12.2	0.274	-4.3 ± 1.9	0.197	23.4
Lip3	DMPC:DPPC:DSPE-PEG_{2000} 40%：55%：5%	199.5 ± 15.3	0.122	-3.9 ± 2.9	0.433	31.7
Lip4	DMPC:DPPC:DSPE-PEG_{2000} 20%：75%：5%	216.5 ± 11.4	0.060	-4.7 ± 3.6	1.689	36.1
Lip5	DPPC:DSPE-PEG_{2000} 95%：5%	196.8 ± 8.8	0.134	-5.8 ± 3.1	0.683	44.4
Lip6	DSPC:DSPE-PEG_{2000} 95%：5%	193.9 ± 13.0	0.166	-2.9 ± 2.9	0.478	54.5

Notes: DOPE is an unsaturated lipid that has a double bond in the hydrophobic chain. The hydrophobic length of the DMPC, DPPC, and DSPC is 14, 16 and 18 carbons, respectively.

Table S2. Characterization of liposomes with different compositions and their diffusivities in rat intestinal mucus

Sample	Composition	Hydrodynamic diameter (nm)	PDI	Zeta potential (mV)	Diffusivity ($\mu m^2/s$)	T_m (°C)	Young's modulus (MPa)
Lip7	PC-98T:DOPE-PEG2000 95%：5%	191.9 ± 12.8	0.156	-2.9	0.156	-17.8	1.3 ± 0.1
Lip8	DMPC:DPPC:DSPC:DSPE-PEG_{2000} 20%：75%：5%	203.6 ± 11.4	0.214	-3.9	1.10	35.9	15.7 ± 1.8
Lip9	HSPC:DSPE-PEG_{2000} 95%：5%	201.8 ± 8.5	0.153	-0.406	0.551	53.2	26.8 ± 2.4

Table S3. Characterization of liposomes with different sizes and their diffusivities in rat intestinal mucus

Sample	Hydrodynamic diameter (nm)	PDI	Zeta potential (mV)	Diffusivity ($\mu m^2/s$)	Ratio of diffusivity
Lip6-80 nm	85.22 ± 8.1	0.151	-2.9 ± 2.9	0.620	1.3
Lip6-200 nm	193.9 ± 13.0	0.166	-2.87 ± 1.4	0.478	1.0
Lip6-300 nm	299.6 ± 3.5	0.260	-3.4 ± 1.5	0.512	1.1
Lip6-400 nm	405.5 ± 1.8	0.166	-2.5 ± 3.9	0.200	0.4
Lip6-500 nm	506.7 ± 2.9	0.151	-3.9 ± 1.7	0.236	0.5
Lip4-200 nm	216.5 ± 11.4	0.060	-4.7 ± 3.6	1.689	3.5

Table S4. The LJ parameters used in simulations

Type1	Type2	$\varepsilon_{lj}(\varepsilon)$	$b(\sigma)$	$r_c(\sigma)$
Liposome	Liposome	0.01	1.0	2.0
	Polymer	0.12	1.0	2.5
	Water	0.1	1.0	3.6
Polymer	Polymer	0.1	1.78	2.0
	Water	0.1	1.0	3.6
Node	Liposome	0.15	2.0	5.0
	Water	0.05	1.0	3.6
Water	Water	0.1	2.7	3.6

Table S5. Parameters used to tune the stiffness of three types of liposomes with low T_m, intermediate T_m, and high T_m.

Type of liposome	μ	$\sin\theta_0$
Low T_m (Lip1)	3.0	0.0
Intermediate T_m (Lip4)	5.0	0.002
High T_m (Lip6)	7.5	0.02

References

1. Yuan H, Huang C, Li J, Lykotrafitis G, & Zhang S (2010) One-particle-thick, solvent-free, coarse-grained model for biological and biomimetic fluid membranes. *Phys Rev E Stat Nonlin Soft Matter Phys* 82(1 Pt 1):011905.

Movie S1. The diffusion and transformation of soft vesicle (liposome with lowest Tm) in hydrogel from molecular dynamics simulation. ($T^*=0.21\varepsilon$).

Movie S2. The diffusion and transformation of hard vesicle (liposome with highest Tm) in hydrogel from molecular dynamics simulation. ($T^*=0.21\varepsilon$).

Movie S3. The diffusion and transformation of simi-rigid vesicle (liposome with medial Tm) in hydrogel from molecular dynamics simulation. ($T^*=0.21\varepsilon$).

Movie S4. The diffusion and transformation of soft vesicles in rat intestinal mucus captured by a gSTED microscope. (T=37 °C)

Movie S5. The diffusion and transformation of hard vesicles in rat intestinal mucus captured by a gSTED microscope. (T=37 °C)

Movie S6. The diffusion and transformation of semi-rigid vesicles in rat intestinal mucus captured by a gSTED microscope. (T=37 °C)